JOURNAL OF GUIDANCE, CONTROL, AND DYNAMICS
Vol. 16, No. 1, January-February 1993

Experimental Study of Robustness in Adaptive Control for Large Flexible Structures

Che-Hang Charles Ih,* David S. Bayard,* Asif Ahmed,† and Shyh Jong Wang*
Jet Propulsion Laboratory, California Institute of Technology, Pasadena, California 91109

An experimental study is performed to investigate the robustness of model reference adaptive control for the large flexible structures control application. The main nonidealities of concern are unmodeled dynamics, input saturation, and time-delay effects (here, actuator and sensor dynamics are lumped into the last item for convenience). This study focuses on the robustness with respect to input saturation and time-delay effects, since robustness to unmodeled dynamics is inherent to the basic algorithm and has been demonstrated experimentally elsewhere.

I. Introduction

AN experimental study is performed to investigate the robustness of model reference adaptive control for the large flexible structures control application. Although adaptive control methods are robust to parametric uncertainty by design, other types of nonidealities are known to lead to degradation and even instability of the closed-loop adaptive system. The main nonidealities of concern in the flexible structures control application are unmodeled dynamics, input saturation, and time-delay effects (here, actuator and sensor dynamics are lumped into the last item for convenience).

Because of the use of the command generator tracker (CGT) approach, the adaptive algorithm considered here achieves tracking objectives that are in theory robust to unmodeled dynamics.[1,2] This theoretical robustness to unmodeled dynamics has also been verified experimentally in Refs. 3 and 4 and will not be an issue in the present study. In contrast, there are presently no assurances as to the stability of the adaptive system to input saturation and time-delay effects. These latter issues will be the focus of the present study.

It is shown experimentally in this paper that the basic adaptive algorithm is robust to input saturation, whereas time-delay effects can cause significant degradation and even instability. It is also shown experimentally that stability in the presence of time delay can be recovered by using a technique advocated by Bar-Kana[5] of placing a small feedforward on the plant (or equivalently for the regulation problem, of placing a small feedback on the compensator). This stabilizes the closed-loop system and recovers a certain degree of performance in the process. As a side benefit, the input torque requirements are also reduced.

Certain theoretical results are included in this paper to support the experimental effort. In particular, it is shown that for structures with collocated actuators and sensors, there always exists a bounded feedforward gain that guarantees L_2 stability of the closed-loop adaptive system in the presence of a pure time delay.

Received July 2, 1990; presented as Paper 90-3498 at the AIAA Guidance, Navigation, and Control Conference, Portland, OR, Aug. 20-22, 1990; revision received Sept. 25, 1991; accepted for publication Feb. 25, 1992.

*Research Scientist. Member AIAA.
†Research Scientist.

II. Adaptive Control Analysis

A. Algorithm Development

The flexible structure dynamics are conveniently written in state space as

$$\dot{x}_p(t) = A_p x_p(t) + B_p u_p(t) \tag{1}$$

$$y_p(t) = C_p x_p(t) \tag{2}$$

where $x_p \in R^{N_p}$, $u_p \in R^M$, $y_p \in R^M$, and A_p, B_p, and C_p are of appropriate dimensions. It is assumed that (A_p, B_p) is controllable, and (A_p, C_p) is observable. Physically, the output y_p is a weighted sum of position and rate measurements, where the position-to-rate ratio is given by α, i.e.,

$$y_p = \alpha y_{\text{pos}} + y_{\text{rate}} \tag{3}$$

A stable reference model that specifies the desired performance of the plant is described by the following state-space representation:

$$\dot{x}_m(t) = A_m x_m(t) + B_m u_m(t) \tag{4}$$

$$y_m(t) = C_m x_m(t) \tag{5}$$

where $x_m \in R^{N_m}$, $u_m \in R^M$, $y_m \in R^M$, and A_m, B_m, and C_m are of appropriate dimensions; u_m is assumed to be a step function.

It is noted that the reference model order N_m can be smaller than the plant order N_p. Define the output error between the plant and model as

$$e_y(t) = y_m(t) - y_p(t) \tag{6}$$

It is desired to adaptively control the plant so that it tracks the model asymptotically at the output

$$\lim_{t\to\infty} e_y(t) = 0$$

The adaptive control is written as

$$u_p = K\tilde{r} \tag{7}$$

where

$$\tilde{r}^T = [\tilde{e}_y^T, x_m^T, u_m^T]^T \tag{8}$$

$$K(t) = [K_e, K_x, K_u] \tag{9}$$

and $\tilde{e}_y$ is the output of the branch filter F_B designed to suppress output noise

$$\tilde{e}_y = F_B e_y \tag{10}$$

The adaptive gain K is chosen as the sum of a proportional and integral component

$$K(t) = K_p(t) + K_I(t) \tag{11}$$

where K_I and K_p are each outputs of linear systems

$$K_I = C_1 X_1 \tag{12}$$

$$\dot{X}_1 = A_1 X_1 + B_1 L e_y \tilde{r}^T T \tag{13}$$

$$K_p = C_2 X_2 \tag{14}$$

$$\dot{X}_2 = A_2 X_2 + B_2 \bar{L} e_y \tilde{r}^T \bar{T} \tag{15}$$

Here, $X_1 \in R^{\eta_2 \times (2M+N_m)}$ and $X_2 \in R^{\eta_2 \times (2M+N_m)}$ are matrix states. Sufficient conditions for global stability are derived in Ref. 2 and are summarized as follows:

1) $T, \bar{T}, L, \bar{L} > 0$.
2) There exists a $P = P^T > 0$ and $Q = Q^T > 0$ such that a) $PB_p = C_p^T$, and b) $PA_p + A_p^T P = -Q$.
3) H_1 and H_2 are strictly positive real (SPR), where

$$H_1(s) = C_1(sI - A_1)^{-1} B_1 L$$

$$H_2(s) = C_2(sI - A_2)^{-1} B_2 \bar{L}$$

4) Rank $\{[C_1 : C_2]\} = M$.
5) $F_B(\cdot)$ is any bounded input/bounded output (BIBO) stable linear or nonlinear filter.

Condition 2 is equivalent to the assumption that the open-loop plant transfer function matrix

$$Z(s) = C_p(sI - A_p)^{-1} B_p \tag{16}$$

is SPR. For a collocated structure having small but nonzero intrinsic damping and no rigid-body modes, this condition can always be satisfied by choosing α in Eq. (3) sufficiently small. The overall adaptive algorithm is depicted in Fig. 1.

Conditions 3 and 4 are satisfied by any SPR filters H_1 and H_2 with nonredundent outputs (i.e., Rank $\{C_1\}$ = Rank $\{C_2\}$ $= M$). For simplicity, they are implemented in the experiment as the following first-order low-pass filters:

$$\dot{K}_I = -\sigma_1 K_I + L e_y \tilde{r}^T T \tag{17}$$

$$\dot{K}_p = -\sigma_2 K_p + \bar{L} e_y \tilde{r}^T \bar{T} \tag{18}$$

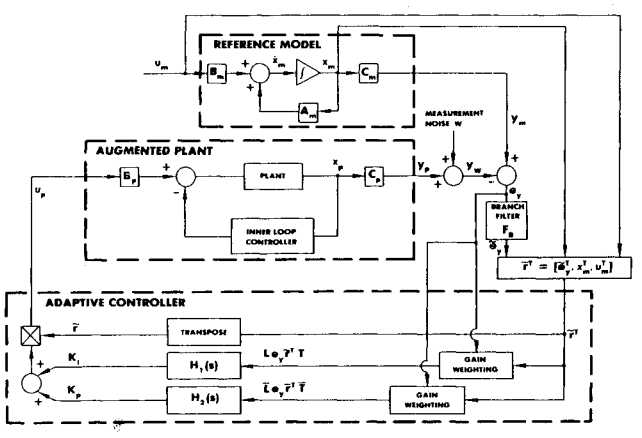

Fig. 1 Adaptive control system block diagram.

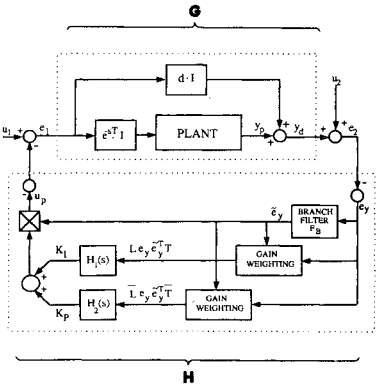

Fig. 2 Block diagram arrangement for passivity analysis (no reference model).

The branch filter F_B is implemented in the experiments as the first-order filter

$$\dot{\tilde{e}} = (e_y - \tilde{e}_y)\gamma \tag{19}$$

B. Robustness to Time Delay

In this section we restrict the discussion to the regulation problem where the reference model is taken as identically zero (i.e., $A_m = 0$, $B_m = 0$, $C_m = 0$). In this case, the block diagram of Fig. 1 can be simplified to that of Fig. 2. However, note that in Fig. 2 the plant has been augmented by a pure delay $e^{-sT_\delta} I$ and feedforward term dI to aid the present discussion. It is of interest to determine to what extent the stability of the adaptive system in the presence of a delay term can be recovered by using a feedforward term. The main result of this section shows that for any bounded delay, there always exists a bounded feedforward term that recovers L_2 stability of the closed-loop adaptive system.

Since a pure time-delay element is infinite dimensional, the stability analysis must be formulated in a Hilbert space setting. For this purpose, the following basic definitions and results on positivity are taken directly from Refs. 6 and 7.

Notation $\mathcal{H}$ is a Hilbert space of real-valued functions (not necessarily scalar-valued) defined on $[0, \infty)$ with scalar product $\langle \cdot, \cdot \rangle$ and corresponding norm $\| \cdot \|$.

Definition 1. Truncation:

Let $x(t)$ be a real, vector-valued function defined on $[0, \infty)$. Define the truncation of $x(t)$ at $t = T$ as

$$x_T(t) = \begin{cases} x(t) & \text{for } 0 \le t \le T \\ 0 & \text{for } t > T \end{cases}$$

Definition 2. Extended Hilbert Space:

$\mathcal{H}_e$ is an extension of $\mathcal{H}$ such that $x \in \mathcal{H}_e$ if and only if $x_T \in \mathcal{H}$ for all $T \in [0, \infty)$. Note that $\mathcal{H} \subset \mathcal{H}_e$.

Definition 3. Causality:

The operator $H: \mathcal{H}_e \to \mathcal{H}_e$ is causal if and only if

$$HX_T = (HX)_T \quad \text{on} \quad [0, T]$$

Theorem 1. Passivity Theorem[6]

Consider the general feedback system of the form

$$e_1 = u_1 - He_2$$

$$e_2 = u_2 + Ge_1 \tag{20}$$

where feedforward block G and feedback block H are operators that map $\mathcal{H}_e$ into $\mathcal{H}_e$. Assume that for any u_1 and u_2 in

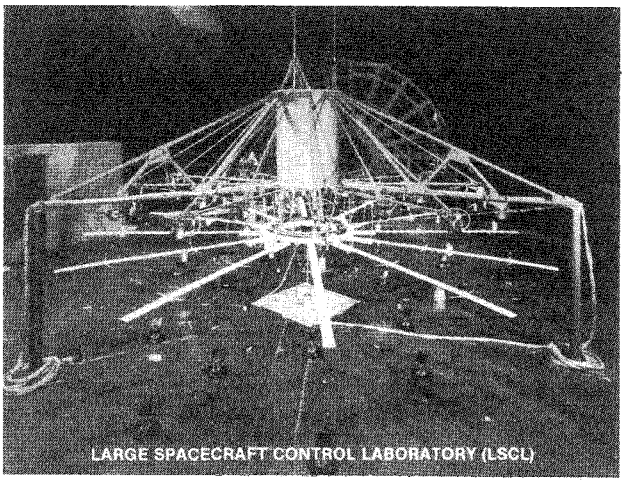

Fig. 3 Experiment structure.

$\mathcal{H}$, there are solutions e_1 and e_2 in $\mathcal{H}_e$. Suppose there are constants γ_1, γ_2, δ, β_1, ϵ, and β_2 such that

$$\|\boldsymbol{G}x\|_T \le \gamma_1\|x\|_T + \gamma_2 \tag{21}$$

$$\langle x, \boldsymbol{G}x\rangle_T \ge \delta\|x\|_T^2 + \beta_1 \tag{22}$$

$$\langle \boldsymbol{H}x, x\rangle_T \ge \epsilon\|\boldsymbol{H}x\|_T^2 + \beta_2 \tag{23}$$

for all $x \in \mathcal{H}_e$, $T \in [0,\infty)$. Under these conditions, if

$$\delta + \epsilon > 0$$

then $u_1, u_2 \in \mathcal{H}$ imply that e_1, e_2, $\boldsymbol{G}e_1$, $\boldsymbol{H}e_2 \in \mathcal{H}$.

Proof: See Ref. 6, page 182.

The foregoing results are now applied to the adaptive system depicted in Fig. 2. The plant transfer function is denoted by $P(s)$ and is assumed to correspond to a structure with collocated torque actuators and position/rate sensors. In particular,

$$P(s) = \sum_{i=1}^{N_p/2} \frac{(s+\alpha)b_i b_i^T}{s^2 + 2\zeta_i\omega_i s + \omega_i^2} \tag{24}$$

where $\omega_i > 0$, $\zeta_i > 0$, $b_i \in R^M$ for all i (i.e., no rigid-body modes and nonzero modal damping). The plant, augmented with both a pure delay and feedforward, is denoted as $G(s)$, where

$$G(s) = dI + e^{-sT_\delta}P(s) \tag{25}$$

with $P(s)$ given by Eq. (24).

Lemma 1

The operator $\boldsymbol{H}$ defined by the adaptation mechanism depicted in Fig. 2 satisfies condition (23) of Theorem 1 for $\epsilon = \beta_2 = 0$, if we assume that $\mathcal{H}$ is the real, vector-valued Hilbert space $L_2[0,\infty)$.

Proof: Construct the positive definite function V such that

$$V = Tr\{T^{-\frac{1}{2}}X_1^T P X_1 T^{-\frac{1}{2}}\} \tag{26}$$

where $P = P^T > 0$, and X_1 is the matrix state defined in Eq. (13). Taking the time derivative and using Eq. (13) gives

$$\dot V = Tr\{T^{-\frac{1}{2}}X_1^T(A_1^T P + PA_1)X_1 T^{-\frac{1}{2}}\} + 2Tr\{T^{-\frac{1}{2}}X_1^T P B_1 L e_y \tilde e_y^T T^{\frac{1}{2}}\} \tag{27}$$

Since $H_1(s)$ in condition 3 is SPR, it follows that there exists a $P = P^T > 0$ and $Q = Q^T > 0$ such that

$$A_1^T P + PA_1 = -Q \tag{28}$$

$$PB_1 L = C_1^T \tag{29}$$

Substituting Eqs. (28) and (29) into (27) gives

$$\dot V = -Tr\{T^{-\frac{1}{2}}X_1^T Q X_1 T^{-\frac{1}{2}}\} + 2Tr\{T^{-\frac{1}{2}}X_1^T C_1^T e_y \tilde e_y^T T^{\frac{1}{2}}\} \tag{30}$$

Using Eq. (12) and a property of the trace operation in Eq. (30) gives

$$\dot V = -Tr\{T^{-\frac{1}{2}}X_1^T Q X_1 T^{-\frac{1}{2}}\} + 2e_y^T K_I \tilde e_y$$

However,

$$0 \le V = \int_0^T \dot V\,dt + V(0) = -\int_0^T Tr\{T^{-\frac{1}{2}}X_1^T Q X_1 T^{-\frac{1}{2}}\}\,dt + 2\int_0^T e_y^T K_I \tilde e_y\,dt + V(0)$$

Assuming that the system is initially at rest gives upon rearranging

$$\int_0^T e_y^T K_I \tilde e_y\,dt \ge \frac{1}{2}\int_0^T Tr\{T^{-\frac{1}{2}}X_1^T Q X_1 T^{-\frac{1}{2}}\}\,dt - \frac{1}{2}V(0) \ge -\frac{1}{2}V(0) = 0 \tag{31}$$

A similar argument can be used to show that

$$\int_0^T e_y^T K_p \tilde e_y\,dt \ge 0 \tag{32}$$

Now, checking condition Eq. (23) of Theorem 1, we have

$$\langle \boldsymbol{H}e_2, e_2\rangle_T = \langle e_y, (K_I + K_p)\tilde e_y\rangle_T = \int_0^T e_y^T K_I \tilde e_y\,dt + \int_0^T e_y^T K_p \tilde e_y\,dt \tag{33}$$

Using Eqs. (31) and (32) in (33) gives

$$\langle \boldsymbol{H}e_2, e_2\rangle_T \ge 0$$

Hence, condition (23) of Theorem 1 is satisfied with $\epsilon = \beta_2 = 0$.

Lemma 2

For any pure delay e^{-sT_δ}, $0 < T_\delta < \infty$, there exists a finite constant $0 \le d < \infty$ such that $\boldsymbol{G}$ defined by Eq. (25) and depicted in Fig. 2 satisfies conditions (21) and (22) of Theorem 1

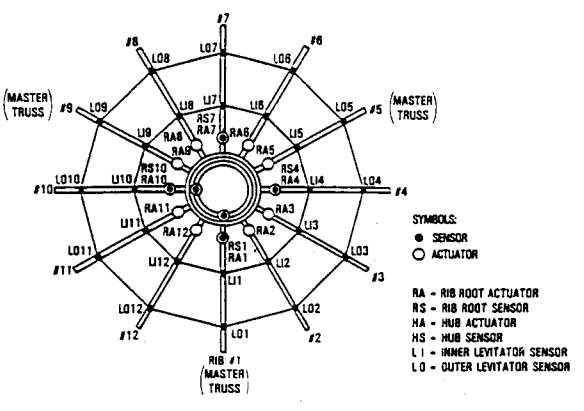

Fig. 4 Bird's-eye view of structure and instrumentation.

for $\gamma_1 > 0$, $\gamma_2 = 0$, $\delta > 0$, and $\beta_1 = 0$ if we assume that $\mathcal{H}$ is the real, vector-valued Hilbert space $L_2[0,\infty)$.

Proof: Rewrite Eq. (25) as

$$G(s) = dI + \tilde{G}(s)$$

where $\tilde{G}(s) = e^{-sT_\delta}P(s)$. Consider the inner product

$$\langle u, Gu\rangle_T = d\|u_T\|^2 + \langle u_T, \tilde{g} \otimes u_T\rangle \tag{34}$$

where $\otimes$ denotes convolution and $\tilde{g}(t)$ is the kernel of the convolution operator associated with $\tilde{G}(s)$. Since $\tilde{G}(s)$ is exponentially stable, it follows that $\tilde{g}(t) \in L_1 \cap L_2$. In addition, since $u_T \in L_2$, we can invoke Parseval's theorem[9] as follows:

$$\begin{aligned}\langle u_T, \tilde{g} \otimes u_T\rangle &= \frac{1}{2\pi}\int_{-\infty}^{\infty} U_T^*(j\omega)\tilde{G}(j\omega)U_T(j\omega)\,d\omega \\ &= \frac{1}{2\pi}\int_{-\infty}^{\infty}\frac{1}{2}U_T^*(j\omega)\left[\tilde{G}(j\omega)+\tilde{G}^*(j\omega)\right]U_T(j\omega)\,d\omega \\ &\geq \frac{1}{2}\inf_\omega \lambda_{\min}\left[\tilde{G}(j\omega)+\tilde{G}^*(j\omega)\right]\frac{1}{2\pi}\int_{-\infty}^{\infty}U_T^*(j\omega)U_T(j\omega)\,d\omega \\ &= \frac{1}{2}\inf_\omega \lambda_{\min}\left[\tilde{G}(j\omega)+\tilde{G}^*(j\omega)\right]\|u\|_T^2 \end{aligned} \tag{35}$$

Combining Eqs. (34) and (35) yields

$$\langle u, Gu\rangle_T \geq \delta\|u\|_T^2 \tag{36}$$

where

$$\delta = d + \frac{1}{2}\inf_\omega \lambda_{\min}\left[\tilde{G}(j\omega)+\tilde{G}^*(j\omega)\right] \tag{37}$$

It is now shown that δ can always be made positive by a suitable choice of $0 \leq d < \infty$. One particular choice is

$$d > \|P\|_\infty \tag{38}$$

This is seen by rearranging Eq. (37) as

$$\begin{aligned}\delta &= d + \frac{1}{2}\inf_\omega \lambda_{\min}\left[\tilde{G}(j\omega)+\tilde{G}^*(j\omega)\right] \\ &= d + \frac{1}{2}\inf_\omega \lambda_{\min}\left[e^{-j\omega T}P(j\omega)+e^{j\omega T}P(-j\omega)\right] \\ &\geq d - \sup_\omega \bar{\sigma}\left[P(j\omega)\right] \\ &= d - \|P(j\omega)\|_\infty > 0 \end{aligned} \tag{39}$$

From Eqs. (36) and (39) it follows that for a choice of d given by Eq. (38), condition (22) of Theorem 1 is satisfied for $\delta = d - \|P\|_\infty$, $\beta_1 = 0$.

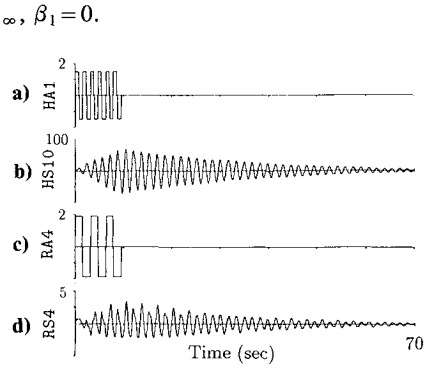

Fig. 5 Open-loop responses: a) hub gimbal axis (HS1), torque (N-M); b) hub gimbal axis (HS10), position (Mrad); c) rib root (RA4), force (N); d) rib root (RS4), position (mm).

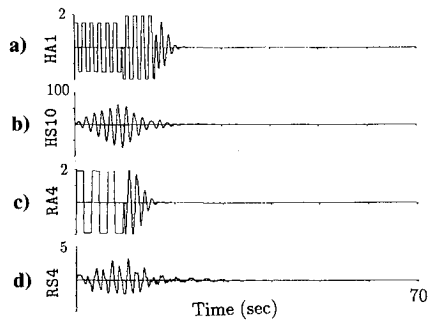

Fig. 6 Closed-loop responses: a) hub gimbal axis (HS1), torque (N-M); b) hub gimbal axis (HS10), position (Mrad); c) rib root (RA4), force (N); d) rib root (RS4), position (mm).

Let $u \in L_{2e}$ and consider the ratio

$$\frac{\|Gu\|_T}{\|u\|_T} = \frac{\|Gu_T\|_T}{\|u_T\|} \leq \frac{\|Gu_T\|}{\|u_T\|} \leq \|G\|_\infty \tag{40}$$

Since $\|G\|_\infty$ is bounded, it follows from Eq. (40) that condition (21) of Theorem 1 is satisfied for $\gamma_1 = \|G\|_\infty$ and $\gamma_2 = 0$.

Theorem 2

For any pure delay e^{-sT_δ}, $0 < T_\delta < \infty$, cascaded with the plant $P(s)$, there exists a bounded feedforward gain dI such that the closed-loop adaptive system depicted in Fig. 2 is L_2 stable.

Proof: From the results of Lemmas 1 and 2, block H (the adaptation mechanism) and block G (plant with delay and feedforward) of Fig. 2 satisfy the conditions of Theorem 1 [i.e., Eq. (21-23), and $\delta + \epsilon > 0$], if we assume that $\mathcal{H}$ is the real, vector-valued Hilbert space $L_2[0,\infty)$.

In summary, there always exists a bounded feedforward term dI such that the closed-loop adaptive system depicted in Fig. 2 is L_2 stabilized (i.e., bounded L_2 input, bounded L_2 output). The practical significance of this result is that the adaptive system can be robustified with respect to time delay by choosing a suitable feedforward gain. Experimental verification of this result will be given in subsequent sections.

III. Experimental Validation

To validate the adaptive control algorithm presented in Sec. II and to study the effects of hardware saturation and time delay on the adaptive controller performance, several experiments were designed and conducted on the JPL/PL Large Spacecraft Control Laboratory (LSCL) Ground Experiment Facility.[8] This facility was built for conducting technology experiments for on-orbit control applications. The experiment facility is an antenna-like structure exhibiting characteristics of large flexible space structures, including densely packed modes, low frequencies, and three-dimensional structural coupling. In this section, the experiment facility, dynamic model, and experiment design are described and experiment results are analyzed and discussed.

A. Experiment Structure and Configuration

A brief overview of the facility will be provided here. A more detailed description can be found in Refs. 3 and 8.

The experiment structure is shown in Fig. 3. It consists of a central circular hub connected to 12 ribs. The ribs are coupled together by two rings of pretensioned wires to provide coupling of motion in the circumferential direction. These coupling wires complicate the dynamics in order to emulate the effect of a simple mesh. The diameter of the structure is 18.5 ft and the ribs are extremely flexible, each supported by two levitators to create the effect of a zero-g environment. The hub is mounted to the backup structure through a gimbal platform so that it is free to rotate about two perpendicular axes in the horizontal plane. A flexible boom is attached to the hub and hangs below it, and a feed mass is attached at the free end of the boom.

Table 1 Normal modes of vibration

Boom-dish modes			
	Frequency, Hz		
Mode no.	Axis 4–10 subsystem	Axis 1–7 subsystem	k
1	0.091	0.091	1
2	0.616	0.628	1
3	1.685	1.687	1
4	2.577	2.682	1
5	4.858	4.897	1
6	9.822	9.892	1

Dish modes		
Mode no.	Frequency, Hz	k
1	0.210	0
2	0.253[a]	2
3	0.290[a]	3
4	0.322[a]	4
5	0.344[a]	5
6	0.351	6
7	1.517	0
8	1.533[a]	2
9	1.550[a]	3
10	1.566[a]	4
11	1.578[a]	5
12	1.583	6
13	4.656	0
14	4.658[a]	2
15	4.660[a]	3
16	4.661[a]	4
17	4.662[a]	5
18	4.663	6
19	9.474	0
20	9.474[a]	2
21	9.474[a]	3
22	9.474[a]	4
23	9.474[a]	5
24	9.474	6

[a]Two-fold degenerate modes.

A bird's-eye view of the structure and associated instrumentation is depicted in Fig. 4. For the hardware saturation and time-delay experiments, the following collocated actuator/sensor pairs are used:

Hub

HA1/HS10
HA10/HS1

Ribs

RA1/RS1
RA4/RS4
RA7/RS7
RA10/RS10

The two hub torquers HAi, $i=1,10$ are linear force actuators that provide torques to the hub by pushing against an inner ring. The torque provided is equal to the force times the lever arm about the axis of rotation. The hub sensors HSi, $i=1,10$ measure angular positions by rotary variable differential transformers (RVDTs) mounted directly on the gimbal axis. Note that each hub sensor measures the structural response to the actuator mounted orthogonal to itself. Hence, although the actuator/sensor pairs HA1/HS1 and HA10/HS10 are physically collocated, it is HA1/HS10 and HA10/HS1 that are collocated in the sense of "dual" variables about a common axis.

The rib root actuators RAi, $i=1,4,7,10$ are solenoid-based designs that provide the desired forces by reacting against the mounts that are rigidly attached to the hub. These actuators are collocated with the four rib root sensors RSi, $i=1,4,7,10$ that measure the linear rib displacements using linear variable differential transformers (LVDTs).

The upgraded computer facility for these experiments is the MicroVax II workstation with the RISC coprocessor. The insertion of the RISC coprocessor board increases the memory of MicroVax II from 5 to 13 MB, and computational speed from 1 to 15 MIPS. This allows us to reduce the sampling period from 45 ms (for the previous two experiments[3,4]) to 25 ms and makes these hardware saturation and time-delay experiments possible.

B. Dynamic Model

A finite element model is developed for the purpose of obtaining a modal model. The boom and each rib are divided into 10 beam-type elements, and the hub is modeled as a very stiff plate. This results in a 308×308 generalized eigenvalue problem to be solved. However, the symmetry of the structure makes it possible to reduce it to a 44×44 problem by separating variables and writing the dependence of the system mode shapes on a circular wave number k.

Mode shapes of the structure can be grouped according to their circular wave number k, which ranges from $k=0$ to $k=6$. Solutions with $k=0$, 2, 3, 4, 5, and 6 are symmetric about the hub, in the sense that all reaction forces on the hub caused by the ribs exactly cancel out. In such modes, which are called "dish modes," neither the hub nor the boom participate in modal motion. On the other hand, modes in which $k=1$ are asymmetric with respect to reaction forces on the hub, these modes called "boom-dish modes," involve motion of the boom, hub, and dish structure together. The lower-frequency modes of the system are listed in Table 1. Note that the modal properties are for the purpose of analysis only, and they are not required for adaptive controller design.

C. Emulated Rate Sensing

Rate measurements are required by this adaptive control algorithm. The facility developed to date does not provide

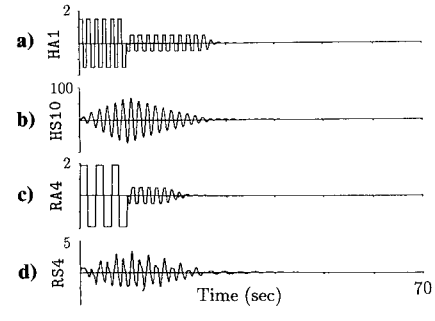

Fig. 7 Closed-loop responses with actuator saturation (threshold = 0.25 T_d): a) hub gimbal axis (HS1), torque (N-M); b) hub gimbal axis (HS10), position (Mrad); c) rib root (RA4), force (N); d) rib root (RS4), position (mm).

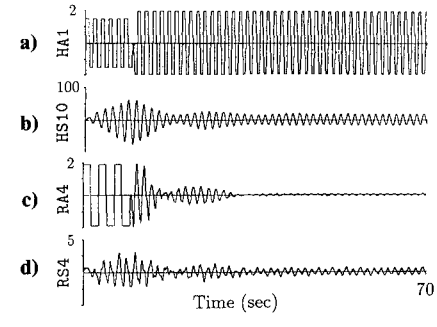

Fig. 8 Closed-loop responses with an eight sampling period delay: a) hub gimbal axis (HS1), torque (N-M); b) hub gimbal axis (HS10), position (Mrad); c) rib root (RA4), force (N); d) rib root (RS4), position (mm).

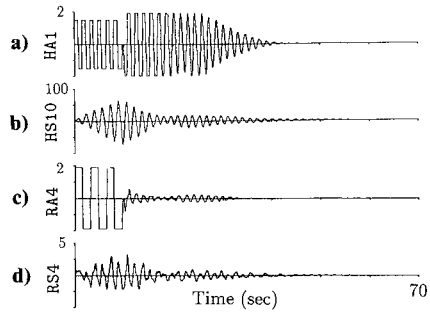

Fig. 9 Closed-loop responses with an eight sampling period delay and feedforward compensation $d \cdot I$ ($d = 0.045$): a) hub gimbal axis (HS1), torque (N-M); b) hub gimbal axis (HS10), position (Mrad); c) rib root (RA4), force (N); d) rib root (RS4), position (mm).

any rate-sensing capability. A Kalman filter (KF) is used as a substitute to estimate the rates from the noisy position measurements. The design of the KF is based on the coarse system description provided by the finite element model. This rate estimation is considered a part of the experiment facility, rather than the adaptive controller.

D. Experiment Design and Results

Three types of transient regulation experiments are designed and conducted in this study. For all of the experiments, the reference model is in a quiescent state, i.e., it has zero input commands and zero initial conditions. A 0.62-Hz pulse train through the hub actuators and a 0.32-Hz pulse train through the rib root actuators are introduced to excite the system for 9.6 s. It is seen from Table 1 that this input simultaneously excites both the boom-dish modes at 0.62 Hz and dish modes at 0.32 Hz. After 9.6 s, the excitation is turned off and the adaptive controller turned on to suppress the resulting vibrations. The controller performance will be compared under nominal conditions (Experiment 1), hardware saturation (Experiment 2), and time-delay (Experiment 3).

Experiment 1 Transient Regulation, Nominal Case

Because of the large number of signals to display in a multivariable application, only some representative ones will be shown and discussed here. The open-loop response to the excitation just mentioned is shown in Fig. 5. Traces (Figs. 5a and 5c) show the input sequences through hub actuator HA1 and rib root actuator RA4, respectively, and traces (Figs. 5b and 5d) show the response of the structure at hub angular sensor HS10 and rib root sensor RS4, respectively. The settling time is 67 s for the hub and 64 s for the rib.

In the closed-loop run, the following choices are made for the adaptive control weightings and parameters:

$$L = \bar{L} = 5 \cdot I$$

$$T = 10^4 \cdot I$$

$$\bar{T} = 6 \cdot I$$

$\sigma_1 = 0.5$ (0.08-Hz integral gain bandwidth)

$\sigma_2 = 21.99$ (3.5-Hz proportional gain bandwidth)

$\gamma = 37.7$ (6-Hz branch filter bandwidth)

$\alpha = 0.0001$

$\tau = 0.025$ s (sampling period)

The closed-loop response to the same excitation is shown in Fig. 6. Traces (Figs. 6a and 6c) are the excitation sequences and control demands, and traces (Figs. 6b and 6d) are the hub and rib root sensor outputs. The limits shown in traces (Figs. 6a and 6c), ± 1.95 N-m and ± 1.95 N, respectively, are the actual actuator torque limits T_d. The settling time drops to 10 s for the hub and drops to 20 s for the rib. The closed-loop response depicted in Fig. 6 establishes the baseline for comparison with subsequent experiments.

Experiment 2 Transient Regulation with Hardware Saturation

To study the effect of hardware saturation, torque limits are imposed on the actuators through software. With the torque and force limits set at ± 0.4875 N-m and ± 0.4875 N (25% of the nominal values T_d), the settling times increase to 22 s for the hub and 23 s for the rib, as shown in Fig. 7. In comparison with the baseline closed-loop response of Fig. 6, it is seen that the performance has degraded in the presence of hardware saturation. However, the degradation is graceful, and the system remains quite stable.

Experiment 3 Transient Regulation with Hardware Time Delay

To emulate the time delay associated with the sensor and actuator dynamics, control signals generated from the adaptive control algorithm are held for several sampling periods using software delay. Two cases are considered: the unmodified adaptive control algorithm and the algorithm with feedforward compensation.

For the unmodified adaptive algorithm, all conditions are kept the same as those of the nominal case, except the control signals are delayed for eight sampling periods. The results are shown in Fig. 8, where it is seen that the effect of the delay is to cause instability.

To compensate for this adverse effect, a feedforward compensation loop is implemented by sending the undelayed control signal to the output, i.e., y_d consists of the position measurement, estimated rate, and undelayed control signal. The feedforward gains selected are $d \cdot I$, where $d = 0.045$. For the eight sampling periods delay case, the compensation restabilizes the system and achieves 35-s settling time for both the hub and rib, as shown in Fig. 9.

E. Discussion

1) It should be emphasized that values for hardware saturation and time delay used in this study are in excess of those already existing on the physical structure.

2) For the regulator problem treated in this paper, the controller is quite robust to actuator saturation. For the tracking problem, however, more recent experience indicates that hardware saturation may interfere with achieving the desired tracking objectives.[10] Analytical expressions developed in Ref. 10 characterize the various contributions to the steady-state tracking error.

3) The actuator time delay can seriously deteriorate the controller performance and even destabilize the system if not properly compensated. The feedforward compensation proposed in Sec. II proved to be quite effective. It not only stabilizes the system, but also recovers performance and reduces input torque requirements.

IV. Conclusions

The experimental study indicates that the basic adaptive algorithm is robust to input saturation, while time-delay effects can cause significant degradation and even instability. It is also demonstrated experimentally that stability in the presence of a time delay can be recovered by placing a small feedforward on the plant. Theoretical support for the latter result is provided by proving that for structures with collocated actuators and sensors, there always exists a bounded feedforward gain that guarantees L_2 stability of the closed-loop adaptive system in the presence of a pure time delay.

Acknowledgments

The research described in this paper was carried out by the Jet Propulsion Laboratory, California Institute of Technol-

ogy, under contract with NASA. The LSCL facility on which the experiments were performed was developed under funding from the U.S. Air Force Phillips Laboratory (formerly, the Rocket Propulsion Laboratory) and NASA Office of Aeronautics and Space Technology.

References

[1]Sobel, K., Kaufman, H., and Mabius, L., "Implicit Adaptive Control Systems for a Class of Multi-Input Multi-Output Systems," *IEEE Transactions on Aeronautical and Electrical Systems,* Vol. AES-18, No. 5, 1982, pp. 576–590.

[2]Bayard, D. S., Ih, C.-H C., and Wang, S. J., "Adaptive Control for Flexible Structures with Measurement Noise," *Proceedings of the American Control Conference* (Minneapolis, MN), Institute of Electrical and Electronics Engineers, Piscataway, NJ, June 10–12, 1987, pp. 368–379.

[3]Ih, C.-H. C., Bayard, D. S., Wang, S. J., and Eldred, D. B., "Adaptive Control Experiment with a Large Flexible Structure," *Proceedings of the AIAA Guidance, Navigation, and Control Conference* AIAA, Washington, DC, 1988; also AIAA Paper 88-4153.

[4]Ih, C.-H. C., Bayard, D. S., Ahmed, A., and Wang, S. J., "Experiments in Multivariable Adaptive Control of a Large Flexible Structure," *Proceedings of the AIAA Guidance, Navigation, and Control Conference,* AIAA, Washington, DC, 1989; also AIAA Paper 89-3571.

[5]Bar-Kana, I., "Robust Simplified Adaptive Control of Large Flexible Space Structures," *Proceedings of the 4th IFAC Symposium on Control of Distributed Parameter Systems* (Univ. of California, Los Angeles, CA), June 30–July 2, 1986.

[6]Desoer, C. A., and Vidyasagar, M., *Feedback Systems: Input-Output Properties,* Academic Press, New York, 1975.

[7]Benhabib, R. J., Iwens, R. P., and Jackson, R. L., "Stability of Large Space Structure Control Systems Using Positivity Concepts," *Journal of Guidance and Control,* Vol. 4, No. 5, 1981, pp. 487–494.

[8]Vivian, H. C., et al., "Flexible Structure Control Laboratory Development and Technology Demonstration," Final Rept. USAF-AFAL/NASA-OAST, JPL Pub. 88-29, Pasadena, CA, Oct. 1987.

[9]Willems, J. C., *The Analysis of Feedback Systems,* M.I.T. Press, Cambridge, MA, 1971.

[10]Boussalis, D., Bayard, D. S., Ih, C.-H. C., Wang, S. J., and Ahmed, A., "Experimental Study of Adaptive Pointing and Tracking for Large Flexible Space Structures," *Proceedings of the AIAA Guidance, Navigation, and Control Conference,* AIAA, Washington, DC, 1991, pp. 769–778; also AIAA Paper 91-2691.